and β' (and not the functions themselves) are strongly increasing functions of r near the TS region, which can be easily seen by differentiating the relevant curves in Figure 4 (see also Figure 10). We can also infer from this that $G_I^{eq\prime}$ is a stronger function of r than is β' because the ionic potential is much more curved. With these observations, we now consider how δ behaves with the solvent polarity. With increasing C, both $G_I^{eq\prime}$ and β' decrease at the transition state, since $r^\ddagger$ diminishes as explained above. Therefore, the denominator $G_C^{eq\prime} - G_I^{eq\prime}$ of δ grows. The numerator behavior with C is not so apparent due to the opposing effects of $G_I^{eq\prime}$ and $-\beta'$. Howeve, since $G_I^{eq\prime}$ is a stronger function of r, $G_I^{eq\prime}/2 - \beta'$ decreases, and so does the numerator. As a result, δ diminishes with C. We thus conclude that the TS ionic character $c_I^{\ddagger 2}$ wanes with increasing solvent polarity.

Registry No. *t*-BuCl, 507-20-0; *t*-BuI, 558-17-8; $Me_4N^+Cl^-$, 75-57-0.

A Theoretical Model for S_N1 Ionic Dissociation in Solution. 2. Nonequilibrium Solvation Reaction Path and Reaction Rate

Hyung J. Kim† and James T. Hynes*

Contribution from the Department of Chemistry and Biochemistry, University of Colorado, Boulder, Colorado 80309-0215. *Received April 3, 1991*

Abstract: The theoretical formulation developed in the preceding article [Kim, H. J.; Hynes, J. T. *J. Am. Chem. Soc.*, preceding paper in this issue] is applied to determine the reaction path and rate constant for the S_N1 ionization process in solution RX $\rightarrow R^+ + X^-$, illustrated for *t*-BuCl. It is found that the intrinsic solution reaction path (SRP), which is the analogue of the familiar minimum energy path of gas-phase reaction studies, differs considerably from the conventionally assumed equilibrium solvation path (ESP). In particular, the SRP near the transition state lies mainly along the RX separation coordinate r. There is little motion in the solvent coordinate s; the solvent lags the solute nuclei motion and there is nonadiabatic nonequilibrium solvation. Near the reactant configuration RX, however, the critical motion initiating the reaction is that of the solvent, i.e., the solvent orientational polarization. The contrasts with activated electron transfer are also pointed out. The connection of the two-dimensional (r, s) free energy surface to the potential of mean force is made, particularly in connection with the ionization activation free energy, as is the connection to the conventional transition-state theory (TST) rate constant k^{TST}, which assumes equilibrium solvation. The deviation of the actual rate constant k from its TST approximation (the transmission coefficient $\kappa = k/k^{TST}$) due to nonequilibrium solvation is examined, via both linear and nonlinear variational transition state theory. Despite the pronounced anharmonicity of the (r, s) free energy surface arising from the electronic mixing of the covalent and ionic valence bond states, a simple harmonic nonadiabatic solvation analysis is found to be suitable. This analysis predicts progressively larger and more significant departures from equilibrium solvation TST with increasing solvent polarity.

1. Introduction

In the preceding article,[1] hereafter referred to as part 1, we have developed a theoretical formulation to describe the unimolecular S_N1 ionization process RX $\rightarrow R^+X^-$ in solution. Our focus there was on the reaction free energetics and the electronic structure of the transition state, features which we examined via an implementation of the theory for a model of *t*-BuCl ionization in a dielectric continuum solvent. In particular, the S_N1 solute electronic structure represented by its wave function Ψ was studied, in a simple two orthonormal valence bond state basis consisting of a covalent state $\psi_C[RX]$ and an ionic state $\psi_I[R^+X^-]$, via

$$\Psi(r,s) = c_C\psi_C[RX] + c_I\psi_I[R^+X^-] \qquad (1.1)$$

where the state coefficients c_C, c_I depend on both the RX nuclear separation coordinate r and the collective solvent coordinate s. (See section 2 and 4A of part 1 for details on this basis set.)

In the present article, we turn our attention to two different aspects of the ionization, namely, the reaction path and the reaction rate constant. For this purpose, we again exploit the theoretical determination of a two-dimensional free energy surface $G(r,s)$ in the RX separation coordinate r and the solvent coordinate s, and again implement the theory for the model of the *t*-BuCl S_N1 ionization described in section 4 of part 1. We examine a wide range of solvent polarity, but often specialize to the three solvents considered in part 1: acetonitrile, chlorobenzene, and benzene.

In the usual conception of the S_N1 ionization, the reaction is pictured as the passage of the reaction system over a barrier in the RX separation r, and the transition-state theory (TST) would be applied to calculate the rate constant as k^{TST} for this process.[2] But as has been described generally for reactions in solution[3] and in particular for the S_N1 process by Zichi and Hynes,[4] and Lee and Hynes,[5a] this usual perspective involving TST assumes that equilibrium solvation holds; in particular, the solvent is supposed to remain completely equilibrated to the RX solute as the RX bond stretches and breaks, and its electronic charge distribution evolves, in the passage through the transition state. But this assumption is in general not valid: the time scale for the response of, e.g., the orientational polarization of the solvent is not sufficiently fast for the solvent to remain so equilibrated. In consequence of these nonequilibrium solvation conditions, the actual reaction path departs from the equilibrium path, and the rate constant differs from its TST approximation. (For general reviews of the extensive recent research on the departure from TST in

† Present address: Dept. of Chemistry, Carnegie Mellon Univ., Pittsburgh, PA 15213-3890.

(1) Kim, H. J.; Hynes, J. T. *J. Am. Chem. Soc.*, preceding paper in this issue.

(2) Ingold, C. K. *Structure and Mechanism in Organic Chemistry*, 2nd ed.; Cornell University Press: Ithaca, NY, 1969. Reichardt, C. *Solvents and Solvent Effects in Organic Chemistry*, 2nd ed.; Verlag Chemie: Weinheim, 1988. Entelis, S. G.; Tiger, R. P. *Reaction Kinetics in the Liquid Phase*; Wiley: New York, 1976.

(3) (a) van der Zwan, G.; Hynes, J. T. *J. Chem. Phys.* **1982**, *76*, 2993. (b) van der Zwan, G.; Hynes, J. T. *J. Chem. Phys.* **1983**, *78*, 4174. (c) van der Zwan, G.; Hynes, J. T. *Chem. Phys.* **1984**, *90*, 21. (d) See also: Hynes, J. T. In *The Theory of Chemical Reaction Dynamics*; Baer, M., Ed.; CRC Press: Boca Raton, FL, 1985; Vol. 4.

(4) Zichi, D. A.; Hynes, J. T. *J. Chem. Phys.* **1988**, *88*, 2513.

(5) (a) Lee, S.; Hynes, J. T. *J. Chem. Phys.* **1988**, *88*, 6863. (b) Lee, S.; Hynes, J. T. *J. Chem. Phys.* **1988**, *88*, 6853.

0002-7863/92/1514-10528$03.00/0

solution, see refs 3d and 6.) These issues have been explored for S_N1 systems in refs 4 and 5, but as noted in section 1 of part 1, the present theory goes beyond those studies by an explicit and proper treatment of the quantum chemical, electronic structural aspects of the ionizing RX solute. As detailed in part 1, these features play a critical role in the reaction. In addition, we explore the influence of a wide range of solvent polarity.

In the present exposition, we rely heavily on the details of the theoretical formulation and model descriptions already given in part 1, and focus attention solely on those features necessary to find and interpret the S_N1 ionization reaction path and rate constant. It is worth remarking that a simplified version of this formalism, but with a microscopic generalization of the solvent coordinate, has now been used to examine these features via molecular dynamics computer simulation.[7] While reaction path analyses are quite common for gas-phase reactions,[8-11] there are very few solution-phase examples. In addition to the S_N1 studies noted above, some studies dealing with aspects of reaction paths for S_N2 reactions in solution may be found in refs 5, 12b, and 12f.

The outline of this paper is as follows. In section 2, we examine the intrinsic solution reaction path and its departure from the conventional equilibrium solvation path. The potential of mean force and the transition-state theory rate constant k^{TST} are examined in section 3. The departures of the rate constant from the equilibrium solvation k^{TST} values due to nonequilibrium solvation are discussed in section 4, while section 5 concludes.

2. Intrinsic and Equilibrium Solvation Reaction Paths

We first study the S_N1 ionization reaction path and compare this with the conventional equilibrium solvation picture for the dissociation. For this purpose, we consider two distinct reaction paths for the ionization on the two-dimensional reaction free energy surface $G(r,s)$ (eq 3.11 of part 1)

$$G(r,s) = V_C^0(r)c_C^2 + [V_I^0(r) - \Delta G_r^{el}(r) - 2\Delta G_r(r)s]c_I^2 - 2\beta(r)c_Cc_I + f\Delta G_r^{el}(r)c_I^2(1 - c_I^2) + \Delta G_r(r)s^2 - k_BT \ln [r/r_0]^2 \quad (2.1)$$

$$f \equiv \rho/(2c_Cc_I + \rho)$$

where $V_C^0(r)$, $V_I^0(r)$ are, respectively, vacuum potentials for the covalent and ionic valence bond states RX and R^+X^- in the orthonormal two state basis $\{\psi_C[RX], \psi_I[R^+X^-]\}$, $\beta(r)$ is the vacuum electronic coupling between the two, and c_C, c_I, which are functions of r and s, are the S_N1 solute state coefficients in eq 1.1. (See section 4A of part 1 for details on the gas-phase t-BuCl diabatic potentials and electronic coupling.) Here $\Delta G_r^{el}(r)$, $\Delta G_r(r)$ are the self-energies associated with the solvent electronic and orientational polarizations (cf. eqs 2.13 and 2.14 of part 1)

$$\Delta G_r(r) = \left(\frac{1}{\epsilon_\infty} - \frac{1}{\epsilon_0}\right)M_s(r)$$
$$\Delta G_r^{el}(r) = \left(1 - \frac{1}{\epsilon_\infty}\right)M_s(r) \quad (2.2)$$

where $M_s(r)$ is the self-energy associated with the vacuum electric field arising from the ionic state charge distribution, determined by its wave function $\psi_I[R^+X^-]$ (eqs 2.9 and 2.10 of part 1). In section 2 of part 1, it is shown that $\Delta G_r^{el}(r)$, $\Delta G_r(r)$ are the reorganization free energies associated, respectively, with the solvent electronic and orientational polarizations when the solute electronic wave function changes abruptly from the ionic to covalent states and vice versa in a Franck–Condon transition. The parameter $\rho = 2\beta/\hbar\omega_{el}$, where ω_{el} is the electronic solvent frequency, determines the character of the equilibration of the solvent electronic polarization to the solute (cf. section 3A of part 1 and ref 13). Finally, the solvent coordinate s in eq 2.1 is a convenient variable, which gauges the nonequilibrium solvent orientational polarization configuration $\vec{P}_{or}$ (eq 2.7 of part 1),

$$\vec{P}_{or} = \frac{1}{4\pi}\left(\frac{1}{\epsilon_\infty} - \frac{1}{\epsilon_0}\right)\epsilon_\infty[s\vec{\mathcal{E}}_I + (1 - s)\vec{\mathcal{E}}_C] \quad (2.3)$$

where ϵ_∞ and ϵ_0 are the optical and static dielectric constants for the solvent, and $\vec{\mathcal{E}}_I$ and $\vec{\mathcal{E}}_C$ are the vacuum electric fields arising from the solute ionic and covalent states, ψ_I and ψ_C, respectively. Thus $s = 1$ corresponds to $\vec{P}_{or}$ equilibrated to the solute ionic state charge distribution, while $s = 0$ denotes the equilibration to the covalent state charge distribution determined by $\psi_C[RX]$. Of course, s values outside this range are possible; for example, $s > 1$ if $\vec{P}_{or}$ exceeds the equilibrium value for the ionic state.

As explained in part 1, the nonequilibrium free energy $G(r,s)$ is obtained by solving a nonlinear Schrödinger equation (eq 3.6 of part 1) for the S_N1 solute wave function Ψ for any given RX separation r and solvent coordinate s. The solvent electronic polarization is assumed to be always in equilibrium with the solute charges and the solvent orientational polarization;[1,13] the solvent orientational polarization, gauged by s, need not be in equilibrium. For illustration, we repeat here the final form of this nonlinear Schödinger equation (cf. eq 3.9 of part 1)

$$2\beta x - [V_I^0 - V_C^0 - \Delta G_r^{el} - 2\Delta G_r s]y = \tfrac{1}{2}\Delta G_r^{el} f(1 + f)xy \quad (2.4)$$

in terms of the localization and delocalization variables x and y defined as

$$x \equiv c_C^2 - c_I^2; \quad y \equiv 2c_Cc_I; \quad x^2 + y^2 = 1 \quad (2.5)$$

The localization variable x gauges the extent of charge localization for the S_N1 solute, while y represents how much it is delocalized; for example, $x = 0$ and $y = 1$ for an equal (thus completely delocalized) mixture of the covalent and ionic states, i.e., $\Psi = (1/\sqrt{2})[\psi_C + \psi_I]$. By solving eq 2.4 for x and y (and thus c_C and c_I) in terms of r and s and substituting into eq 2.1, we can explicitly determine the two-dimensional reaction system free energy $G(r,s)$ and examine the possible reaction routes for S_N1 ionization.

The first of these is the equilibrium solvation path (ESP) introduced in section 3B of part 1, defined by

$$\partial G(r,s)/\partial s = 0 \quad (2.6)$$

and illustrated in Figure 1 for t-BuCl in acetonitrile and chlorobenzene solvents. Along this path the solvent orientational polarization configuration is such that the resulting free energy is always minimum for any given r. Thus the solvent polarizations (both electronic and orientational) maintain full equilibrium with the solute charges along the ESP. It has been already pointed out in section 3B of part 1 that along the ESP, the relation

$$s = s_{eq} = c_I^2 \quad (2.7)$$

(6) Truhlar, D. G.; Hase, W. L.; Hynes, J. T. *J. Phys. Chem.* **1983**, *87*, 2664. Hynes, J. T. *Annu. Rev. Phys. Chem.* **1985**, *36*, 573. Berne, B. J.; Borkovec, M.; Straub, J. E. *J. Phys. Chem.* **1988**, *92*, 3711. Hänggi, P.; Talkner, P.; Borkovec, M. *Rev. Mod. Phys.* **1990**, *62*, 251. Whitnell, R. M.; Wilson, K. R. *Rev. Comp. Chem.*, in press.

(7) Keirstead, W.; Wilson, K. R.; Hynes, J. T. *J. Chem. Phys.* **1991**, *95*, 5256.

(8) Fukui, K. *J. Phys. Chem.* **1970**, *74*, 4161; *Acc. Chem. Res.* **1981**, *14*, 363.

(9) Miller, W. H.; Handy, N. C.; Adams, J. E. *J. Chem. Phys.* **1980**, *72*, 99. Miller, W. H. *J. Phys. Chem.* **1983**, *87*, 3811.

(10) For a recent exposition, see, e.g.: Melissas, V.; Truhlar, D. G.; Garrett, B. C. *J. Chem. Phys.* **1992**, *96*, 5758 and references therein.

(11) Miller, W. H. *J. Chem. Phys.* **1976**, *65*, 2216. Pechukas, P. *Annu. Rev. Phys. Chem.* **1981**, *32*, 159. Garrett, B. C.; Truhlar, D. G.; Grev, R. S. In *Potential Energy Surfaces and Dynamics Calculations*; Truhlar, D. G., Ed.; Plenum: New York, 1981. Truhlar, D. G. *Annu. Rev. Phys. Chem.* **1984**, *35*, 159. Hase, W. L. *Acc. Chem. Res.* **1983**, *16*, 258. Pollak, E. In *The Theory of Chemical Reaction Dynamics*; Baer, M., Ed.; CRC Press: Boca Raton, FL, 1985; Vol. 3.

(12) (a) Bergsma, J. P.; Gertner, B. J.; Wilson, K. R.; Hynes, J. T. *J. Chem. Phys.* **1987**, *86*, 1356. (b) Gertner, B. J.; Bergsma, J. P.; Wilson, K. R.; Lee, S.; Hynes, J. T. *J. Chem. Phys.* **1987**, *86*, 1377. (c) Gertner, B. J.; Wilson, K. R.; Hynes, J. T. *J. Chem. Phys.* **1989**, *90*, 3537. (d) Gertner, B. J.; Whitnell, R. M.; Wilson, K. R.; Hynes, J. T. *J. Am. Chem. Soc.* **1991**, *113*, 74. (e) Huston, S. E.; Rossky, P. J.; Zichi, D. A. *J. Am. Chem. Soc.* **1989**, *111*, 5680. (f) Tucker, S. C.; Truhlar, D. G. *J. Am. Chem. Soc.* **1990**, *112*, 3347.

(13) Kim, H. J.; Hynes, J. T. *J. Chem. Phys.* **1992**, *96*, 5088.

holds, and thus, along the ESP, s measures the ionic state occupation probability c_I^2 for the solute wave function Ψ, i.e., the ionic character of the S_N1 solute. Along this path, the free energy is $G_{eq}(r)$ (cf. section 3B of part 1)

$$G_{eq} = V_C^0 c_C^{eq2} + V_I^0 c_I^{eq2} - k_B T \ln [r/r_0]^2 - 2\beta c_C^{eq} c_I^{eq} + \Delta G_{solv}^{eq} \tag{2.8}$$

where the equilibrium solvation free energy $\Delta G_{solv}^{eq}(r, c_I^{eq})$ is given by

$$\Delta G_{solv}^{eq} = (1 - f^{eq})\Delta G_{solv,BO}^{eq} + f^{eq}\Delta G_{solv,SC}^{eq}$$

$$f^{eq} = \frac{\rho}{2c_C^{eq}c_I^{eq} + \rho}$$

$$\Delta G_{solv,BO}^{eq} = -\Delta G_r^{el} c_I^{eq2} - \Delta G_r c_I^{eq4} = -\left(1 - \frac{1}{\epsilon_\infty}\right) M_s c_I^{eq2} - \left(\frac{1}{\epsilon_\infty} - \frac{1}{\epsilon_0}\right) M_s c_I^{eq4}$$

$$\Delta G_{solv,SC}^{eq} = -[\Delta G_r^{el} + \Delta G_r] c_I^{eq4} = -\left(1 - \frac{1}{\epsilon_0}\right) M_s c_I^{eq4} \tag{2.9}$$

c_C^{eq}, c_I^{eq} are the r-dependent state coefficients for the S_N1 solute equilibrium solvation wave function in the two-state basis.

The second route is the intrinsic reaction path introduced by Fukui for gas-phase systems,[8] and generalized to reactions in solution by Lee and Hynes.[5b] It is a steepest descent, zero kinetic energy, path from the transition state to the reactant and product states given by the solution of

$$\frac{\mu_r dr}{\partial G/\partial r} = \frac{\mu_s ds}{\partial G/\partial s} \tag{2.10}$$

where the μ's are the masses associated with the solute nuclear separation and the solvent. This will be termed the *solution reaction path* (SRP).[5] Once the appropriate masses are defined, the SRP is[5b] the direct analogue of the minimum free energy path extensively employed in gas-phase studies.[8-10] We stress here that along the SRP, the solvent orientational polarization is in general out of equilibrium, and in consequence the equilibrium relation $s = c_I^2$ does not hold—in this restricted sense, the solvent polarization and the solute electronic structure are decoupled. Here we are dealing with nonequilibrium stationary states[13,14] and nonequilibrium solvation.

Upon rearranging the above equation, we obtain the instructive relation

$$\frac{\partial G/\partial s}{\partial G/\partial r} = \frac{\mu_s ds}{\mu_r dr} \tag{2.11}$$

In the limit $\mu_s \to 0$, the right-hand side vanishes (except in the special case, not encountered here, where ds/dr diverges). Then $\partial G/\partial s$ vanishes and eq 2.10 reduces to eq 2.6. Thus in the vanishing solvent mass limit, the ESP and SRP coincide and equilibrium solvation always applies. In actual solvents, the solvent is not so compliant: the mass $\mu_s(r)$ associated with the solvent orientational polarization is finite. $\mu_s(r)$ (cf eq 3.6 below) is proportional to the solvent reorganization free energy $\Delta G_r(r)$;[5b] it thus increases with the separation r, since the solute charge separation and dipole moment increase as t-BuCl becomes more ionic.[4,5] The more strong is the polar solvent-reacting solute interaction, the more massive the solvent appears to be. For μ_r, we use the reduced mass of *tert*-butyl and chlorine. The calculated reaction paths are plotted in Figure 1 for CH_3CN and C_6H_5Cl solvents.[15]

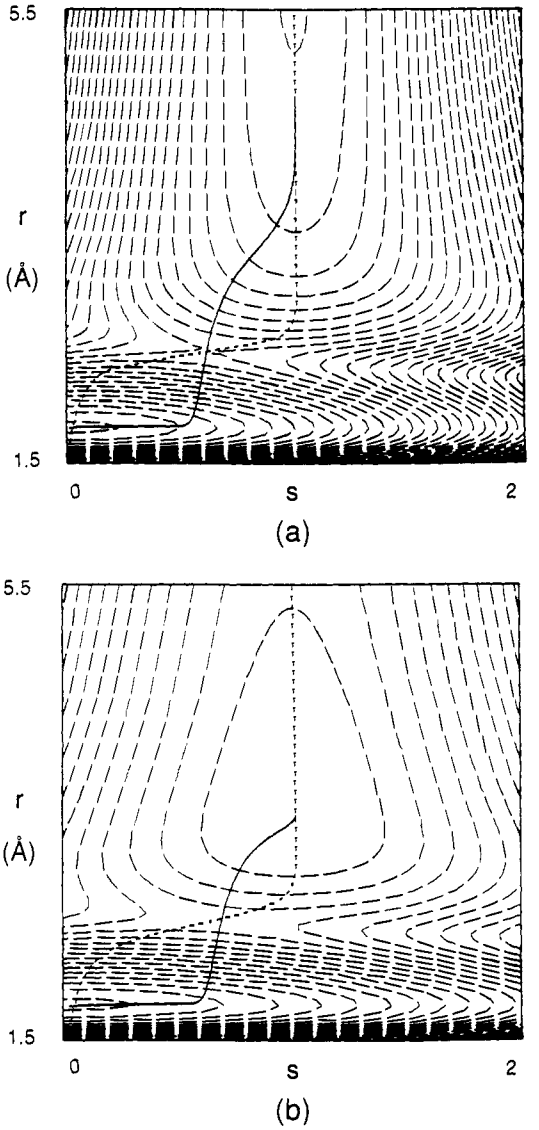

Figure 1. Free energy contour maps for t-BuCl in (a) CH_3CN and (b) C_6H_5Cl solvents. —— denotes the equi-free energy lines. The free energy difference between two nearby contour lines is 0.1 eV (=2.3 kcal/mol). For reference, the free energy value for the contour located in the upper center map (a) is −3.1 eV while that for the closed contour in the center of map (b) is −2.5 eV: (—) solution reaction path (SRP), (- - -) equilibrium solvation path (ESP). The displayed coordinates are not mass-weighted.[5b]

For each solvent case, the two different reaction paths coincide only at the three equilibrium solvation states, viz., the reactant, product, and transition states; except for these three states, the SRP deviates markedly from the ESP. Near the transition state, the direction of the SRP is almost parallel to r, while for the ESP it is nearly perpendicular; in the latter, the equilibrated solvent coordinate $s_{eq}(r) = c_I^2$ changes strongly as the solute ionic character evolves with changing r. This pronounced disparity indicates that the reaction takes place in a "frozen solvent" nonadiabatic solvation environment;[3,5,12] the barrier crossing takes place almost completely in the r-direction, with the solvent acting as a spectator rather than as the coupled rearranging partner envisioned in the ESP. This solvent lag is an illustration of lack of synchronization in a reaction context.[16] This lag can be understood as follows.[3] Since the barrier is rather sharp, it takes only a short time to cross the barrier in the r direction. During this brief barrier crossing epoch, the comparatively sluggish solvent cannot follow the rapid change in the solute. Thus the solvent orientational polarization is almost

(14) In the context of self-consistent field approximation, see: (a) Kim, H. J.; Hynes, J. T. *J. Chem. Phys.* **1990**, *93*, 5194. (b) Kim, H. J.; Hynes, J. T. *J. Chem. Phys.* **1990**, *93*, 5211. (c) Kim, H. J.; Hynes, J. T. *J. Phys. Chem.* **1990**, *94*, 2736. (d) Kim, H. J.; Hynes, J. T. *Int. J. Quantum Chem. Symp.* **1990**, *24*, 821.

(15) As noted in section 4B of part 1, there is no solvent coordinate in the case of nonpolar benzene solvent, since there is no orientational polarization.

(16) Bernasconi, C. F. *Adv. Phys. Org. Chem.* **1992**, *27*, 119; *Acc. Chem. Res.* **1992**, *25*, 9.

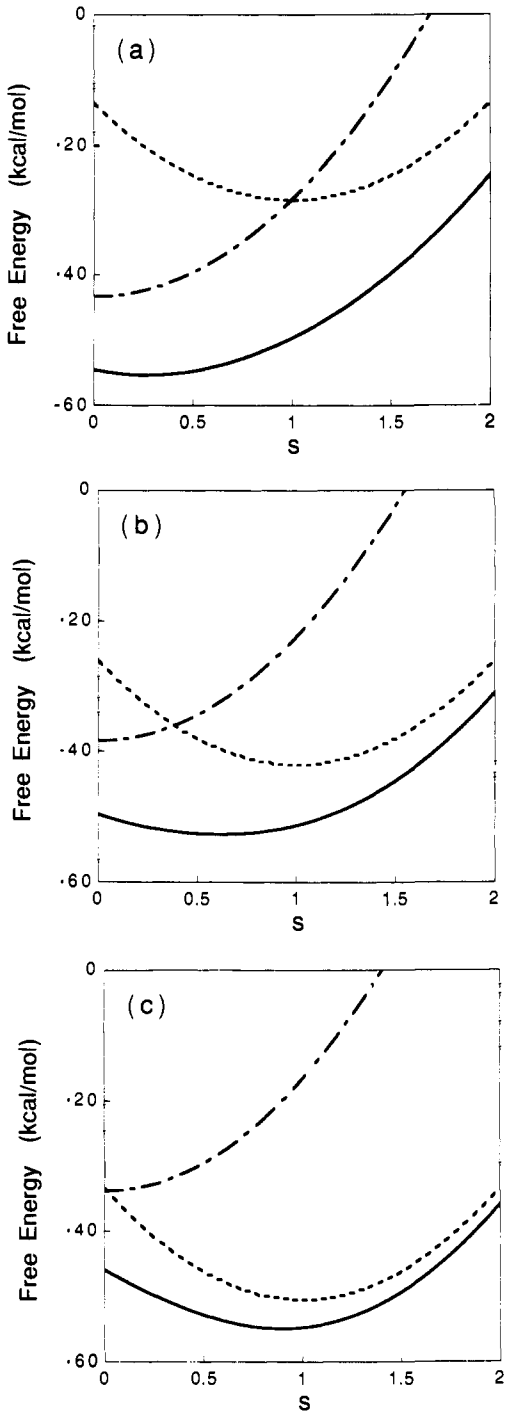

Figure 2. Free energy profile along the solvent coordinate s in acetonitrile solvent: (a) $r \approx 2.37$ Å; (b) $r \approx 2.47$ Å; (c) $r \approx 2.57$ Å: (—) ground state, (- - -) covalent state, (···) ionic state.

frozen during the barrier crossing, creating a static nonequilibrium environment for the reaction. While it is possible for this frozen environment to produce a caging potential along r,[3b,c] in the present case the decrease in the potential along r outweighs any increase due to solvation disequilibrium, and no caging effect results.

It is worth pausing to observe that it is often expressed in the literature that there is no, or little, solvent component in the reaction coordinate in the equilibrium solvation regime. But this is not correct and is, in fact, the precise *opposite* of the state of affairs, as evidenced in Figure 1 and discussed extensively elsewhere.[3-5,12,17] For when equilibrium solvation holds, the solvent

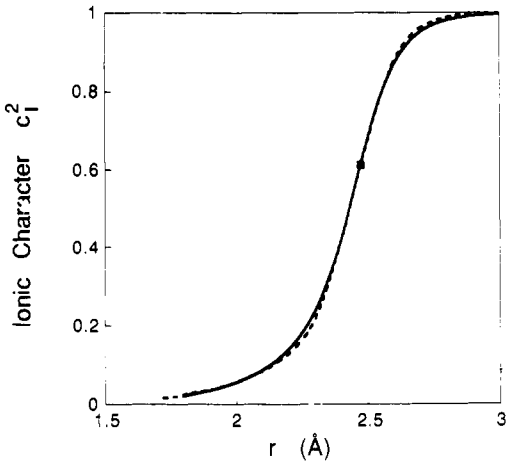

Figure 3. Charge distributions along SRP and ESP in CH_3CN (cf. Figure 7 of part 1): (—) SRP, (- - -) ESP. The filled square denotes the transition state. The charge distributions for the two reaction paths differ only slightly, although the actual paths in the (r, s) reaction coordinates differ rather markedly. This reveals that the ionic state occupation c_I^2 and the solvent coordinate s are not in general related along the SRP, while the relation $s = c_I^2$ holds along the ESP.

molecules must move to maintain equilibrium with the evolving charge distribution and nuclear configuration of the reactive solute as it passes across the transition state.

Now we turn to the situation near the reactant state. Here we find (cf. Figure 1) that by contrast to the transition-state region, the SRP is almost exclusively along the solvent coordinate s up to ≈4 kcal/mol in the case of acetonitrile, which is almost 15% of the total activation free energy. According to this reaction picture, the solvent orientational polarization fluctuations constitute the most important factor in *initiating* the ionic dissociation in solution. When the initial $\bar{P}_{or}$ fluctuations take the system to an energetically favorable configuration for the barrier crossing, the nuclear motion in r begins to appear and brings the system over the barrier while $\bar{P}_{or}$ is essentially fixed.[18] A similar phenomenon has been observed in a detailed molecular dynamics computer simulation of the ascent to the transition state for the $Cl^- + CH_3Cl$ S_N2 reaction in water.[19]

As regards the product state, we notice a striking difference between highly polar CH_3CN and weakly polar C_6H_5Cl; the product state for CH_3CN solvent corresponds to completely dissociated ions $R^+ + X^-$ (i.e., $r \to \infty$, $s = 1$), while that for C_6H_5Cl is an ion pair R^+X^- located at $r \approx 3.44$ Å and $s \approx 1$, indicated by the local minimum in Figure 1b. Thus our dielectric continuum model predicts a dissociation into ion pairs in weakly polar solvents; some perspectives on this are given in section 4B of part 1.

Finally, the above barrier passage at fixed $\bar{P}_{or}$ and thus s values is more than a little reminiscent of electron-transfer reactions.[20,21] But the S_N1 reaction is nonetheless quite different in character from an activated electron transfer. For consider the free energy profile along the solvent coordinate s with fixed r. The free energy curves for the ground state and the two diabatic covalent and ionic states for t-BuCl in acetonitrile solution along s, which passes through the transition state ‡, are plotted in Figure 2. The essential point is that the ground electronic state is characterized

(17) Ciccotti, G.; Ferrario, M.; Hynes, J. T.; Kapral, R. *J. Chem. Phys.* **1990**, *93*, 7137.

(18) The SRP is a limiting zero kinetic energy path,[5,8] and therefore does not include vibrational oscillations of the (mainly) covalent t-BuCl reactant. To be sure, such motions occur in the dynamics, and reactant vibrational excitation will be important in the S_N1 reaction,[7] as it is in, e.g., the S_N2 reaction.[12a,d]

(19) Gertner, B. J.; Whitnell, R. M.; Wilson, K. R.; Hynes, J. T. *J. Am. Chem. Soc.* **1991**, *113*, 74.

(20) Marcus, R. A. *J. Chem. Phys.* **1956**, *24*, 966, 979; *Faraday Discuss. Chem. Soc.* **1960**, *29*, 21; *J. Chem. Phys.* **1963**, *38*, 1858; *Annu. Rev. Phys. Chem.* **1964**, *15*, 155.

(21) For some general reviews, see: Sutin, N. *Prog. Inorg. Chem.* **1983**, *30*, 441. Newton, M. D.; Sutin, N. *Annu. Rev. Phys. Chem.* **1984**, *35*, 437. Marcus, R. A.; Sutin, N. *Biochim. Biophys. Acta* **1985**, *811*, 265.

by a single stable well potential, a point also stressed in part 1. This is in complete contrast to activated electron-transfer reactions, where there is a solvent barrier in s; in the language of Pross and Shaik,[22] we would say that there is an electron shift rather than an electron transfer. Thus the t-BuCl S_N1 reaction corresponds to the strong electronic coupling limit,[14a,b,d] where the relatively large electronic coupling (≈13–18 kcal/mol at the transition state) obliterates the solvent barrier completely.[23] The contrast with electron-transfer reactions can be heightened by considering Figure 3. While the charge separation development is certainly rapid in the internuclear separation r as the t-BuCl ionic character develops, it nonetheless does not at all have the abrupt Franck–Condon isoenergetic character associated with pure electron transfer (see, e.g., ref 21). Instead there is a considerable free energy change of order 10 kcal/mol which accompanies the change in r associated with the major change in the ionic character. Thus the S_N1 charge development is strongly coupled to the geometric change in r, although not in a linear[24] fashion.

3. Potential of Mean Force and Transition State Theory Rate Constant

In our discussion to date, including that of part 1, we have used a two-dimensional (r,s) perspective to discuss, e.g., activation free energies and transition-state locations. But this is a perspective not available from conventional equilibrium statistical mechanical approaches to activation free energetics,[25] which are intrinsically one dimensional in character. Nor is it available from experimental rate studies, in which activation free energies are inferred, in the main, from transition-state theory. In this section, we forge the connection of our treatment to both these approaches. We have already described the equilibrium solvation path ESP above, along which the free energy is $G_{eq}(r)$. Several examples of this were given in section 4B of part 1 and used to locate the transition state, as well as stable reactants and products. Here we describe first the connection of that free energy to the conventional object of equilibrium statistical mechanical calculation and simulation—the potential of mean force. We then pass to the transition-state theory rate constant, which is most naturally expressed in terms of free energy differences connected to this potential of mean force. To anticipate a major conclusion of this section, we will find that our previous location of the transition state here and in part 1 is confirmed.

At any given r, along the solvent coordinate s, the nonequilibrium free energy $G(r,s)$ near equilibrium solvation states can be written in the harmonic approximation as[14]

$$G(r,s) = G_{eq}(r) + \tfrac{1}{2}K_s(r)\delta s^2 \qquad (3.1)$$

where δs is the deviation from the equilibrium solvation value $s_{eq}(r)$, eq 2.7. The solvent force constant K_s, which measures the restoring ability of the solvent when it deviates from equilibrium solvation $s_{eq}(r)$, can be obtained by taking the second derivatives of nonequilibrium free energy $G(r,s)$ (eq 2.1) with respect to s,

$$K_s(r) \equiv \left.\frac{\partial^2 G}{\partial s^2}\right|_{eq} = 2\Delta G_r(r)\left[1 + \frac{1}{2}\frac{\partial x(r,s)}{\partial s}\right]_{eq} = K_s^0(r)\left[1 + \frac{1}{2}\frac{\partial x(r,s)}{\partial s}\right]_{eq} \qquad (3.2)$$

where the derivatives are evaluated at equilibrium solvation. In view of eq 2.5, we can see easily that $\partial x/\partial s$ in eq 3.2 arises from the solute electronic structure change with the solvent coordinate s (and thus the solvent orientational polarization). The zeroth-order solvent force constant $K_s^0(r)$, where the solute electronic structure change is neglected, is given by twice the solvent reorganization free energy $2\Delta G_r(r)$.[26,27] (The calculation of $\Delta G_r(r)$ is outlined in part 1, eqs 4.6–4.8 with eq 2.13.) In section 5C of part 1, $\Delta G_r(r)$ has also been related to the (in principle) experimentally measurable thermodynamic quantity, i.e., the free energy of transfer for an ion pair, separated by a distance r (eq 5.12 of part 1).

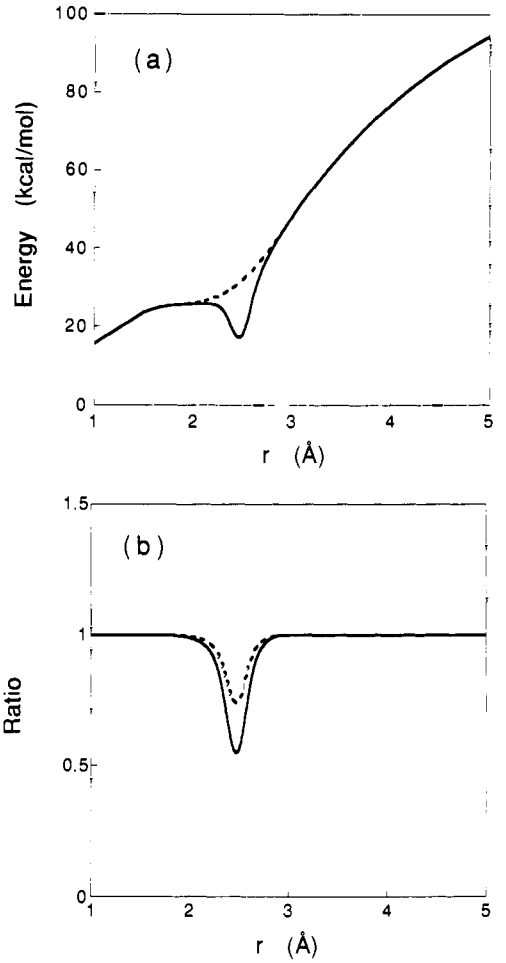

Figure 4. (a) Solvent force constant: (—) $K_s(r)$, (···) $2\Delta G_r(r)$. The solvent mass $\mu_s(r)$, which is proportional to $\Delta G_r(r)$, thus increases smoothly and monotonically with r. (b) Solvent frequency and force constant ratio: (—) $K_s/2\Delta G_r$, (···) ω_s/ω_s^0.

For acetonitrile, $K_s(r)$ is plotted in Figure 4a. Because of the very strong solvent-induced mixing between the pure covalent and ionic valence bond states of t-BuCl near the transition state, K_s deviates significantly from $2\Delta G_r$, e.g., at the transition state $K_s/2\Delta G_r \approx 0.55$. Thus the actual solvent force constant at the transition state is smaller than the zeroth order value by a factor of about 2; in a sense, this is a "critical" intermediate point for the reaction where solvent fluctuations are large.[28] (A similar reduction is observed in the MD study of ref 7.) Since the solvent mass $\mu_s(r)$ defined by the equipartition theorem

$$\langle \delta s^2(r) \rangle = k_B T/\mu_s(r) \qquad (3.3)$$

(22) Pross, A.; Shaik, S. S. *Acc. Chem. Res.* **1983**, *16*, 363.
(23) For weakly-coupled t-BuI, however, the solvent barrier persists. See: Mathis, J. R.; Kim, H. J.; Hynes, J. T. To be submitted for publication.
(24) Pross, A. *Adv. Phys. Org. Chem.* **1985**, *21*, 99.
(25) Some simulation and theoretical studies include: Jorgensen, W. L.; Buckner, J. K.; Huston, S. E.; Rossky, P. J. *J. Am. Chem. Soc.* **1987**, *109*, 1891. Morita, T.; Ladanyi, B. M.; Hynes, J. T. *J. Phys. Chem.* **1989**, *93*, 1386. See also the extensive references listed in ref 17.
(26) A difficulty with a continuum model for water solvent is that the continuum solvent force constant (eq 3.2 for K_s^0) has an incorrect (increasing) trend as the t-BuCl ionizes (cf. refs 7 and 27). For a recent discussion of this force constant for ions in water, see: Fonseca, T.; Ladanyi, B. M.; Hynes, J. T. *J. Phys. Chem.* **1992**, *96*, 4085.
(27) Carter, E. A.; Hynes, J. T. *J. Phys. Chem.* **1989**, *93*, 2184.
(28) In Appendix B of ref 14b, the renormalization of the solvent force constant $K_s(r)$, which arises from the mixture of the solute electronic states, has been discussed and related to the solute molecular polarizability. Near the transition state, this polarizability is large (i.e., the covalent and ionic states mix easily), so that the solute electronic charge distribution adjusts to the fluctuating solvent orientational polarization relatively easily compared to the reactant or product states. This solute adjustment, in turn, provides an environment favorable for the solvent to fluctuate. This explains why the solvent force constant is considerably smaller at the transition state.

at fixed r for the solvent velocity $\delta\dot{s}$ is proportional to $\Delta G_r(r)$ (Figure 4a),[5b] the corresponding solvent frequency defined as $\omega_s(r) = \sqrt{K_s(r)/\mu_s(r)}$ becomes

$$\frac{\omega_s(r)}{\omega_s^0} = \left[\frac{K_s(r)}{2\Delta G_r(r)}\right]^{1/2} = \left[1 + \frac{1}{2}\frac{\partial x(r,s)}{\partial s}\right]_{eq}^{1/2} \quad (3.4)$$

where ω_s^0 is the zeroth-order diabatic solvent frequency; i.e., for a diabatic state in the absence of the quantum coupling

$$\omega_s^0 = \sqrt{2\Delta G_r(r)/\mu_s(r)} \quad (3.5)$$

which is itself *independent* of r.[5b] Notice that for any given ω_s^0, the solvent mass $\mu_s(r)$

$$\mu_s(r) = 2\Delta G_r(r)/\omega_s^{0^2} \quad (3.6)$$

grows in proportion to $\Delta G_r(r)$. Here we employ $\omega_s^0 = 15$ ps^{-1}.[5a,29] Near the transition state, the solvent frequency is considerably lower than ω_s^0 by almost a factor of 1.5 (see Figure 4b). This is purely a quantum mechanical electronic structure effect. The extent of the electronic mixing between the two states $\psi_{C,I}$ in the ground state varies with r since the relative mixing is determined by the difference in the diabatic energies $V_{C,I}^0$, the coupling β, and the reorganization energies ΔG_r^{el}, ΔG_r, all of which change with r. This differing mixing is completely missing in the classical analysis[3-5] which prescribed the charge variation as a function of r, and is not properly taken into account in early quantum treatments.[30]

We now proceed to determine the equilibrium potential of mean force $\bar{G}_{eq}(r)$. This one-dimensional perspective, defined solely on the r coordinate and inextricably based on equilibrium solvation ideas,[3] provides a standard statistical mechanical approach to locating the transition state.[3d,6,25] (A discussion of its limitations will be postponed until section 4.) $\bar{G}_{eq}(r)$ can be obtained in the following steps. First, equilibrium solvation is assumed for every RX separation r so that the free energy (minus the solvent fluctuations) in r, $G_{eq}(r)$, is the free energy along the ESP, as in Figure 1, projected onto the r coordinate. Explicit examples are given in Figure 6 of part 1. The solvent fluctuations enter via a solvent well $K_s(r)\delta s^2/2$ at every r in the transverse direction, i.e., eq 3.1. In particular, $\bar{G}_{eq}(r)$ can be written as

$$\begin{aligned}\bar{G}_{eq}(r) &= G_{eq}(r) - k_BT \ln Q_s(r) \\ &= G_{eq}(r) - k_BT \ln\left[\frac{k_BT}{\hbar\omega_s(r)}\right] \end{aligned} \quad (3.7)$$

with $\hbar$ being Planck's constant divided by 2π, where the second term arises from the partition function $Q_s(r)$ for the solvent. In particular, $\omega_s(r)$ is the frequency associated with the solvent motion at fixed RX separation r, eq 3.4, and as discussed below is related to a solvent entropy effect. Because of the electronic coupling between the covalent and ionic states, $\omega_s(r)$ varies with r as shown above.

In order to determine the conventional transition state, defined as the maximum in the potential of mean force, we look for the maximum in $\bar{G}_{eq}(r)$. Since the solvent frequency depends on r and in particular is smaller near the transition-state region, the maximum points in $\bar{G}_{eq}(r)$ and $G_{eq}(r)$ may not coincide, because of the extra temperature-dependent entropic effect associated with the inhomogeneity in $\omega_s(r)$. This is an important question to consider, for recall that $G_{eq}(r)$ was employed in establishing S_N1 ionization activation free energies in sections 4B and 5 of part 1. To be more specific, since $\omega_s(r)$ near the $G(r,s)$ saddle point $r = r^*$ is considerably smaller (Figure 4b), because of the quantum mixing of the covalent and ionic states, the second term in eq 3.7 is correspondingly larger, reflecting a greater entropy associated with a wider "pass" in the s coordinate; it thus reduces $\bar{G}_{eq}(r)$ more near r^* than for other values of r. If this effect were to be significant, then the maximum location for $G_{eq}(r)$ need not be the same as that for $\bar{G}_{eq}(r)$. However, our numerical calculations for both polar solvents show that, at room temperature, the r dependence in $\omega_s(r)$ does in fact *not* induce any significant shift, less than 0.01 Å; the same is true over the temperature range ($\lesssim$350 K) where most solvents remain liquid. This important feature ensures that the transition state obtained from $\bar{G}_{eq}(r)$ coincides with the saddle point in the two-dimensional surface $G(r,s)$ as far as the r-coordinate values are concerned.

The conventional transition-state theory (TST) rate constant would then be the one-way equilibrium flux $\langle j^+\rangle_R$ across r^*, normalized by the reactant-state partition function.[31] This yields

$$\begin{aligned} k^{TST} &= \langle j^+\rangle_R \\ &= \frac{k_BT}{\hbar}\frac{Q_s(r^*)}{Q_{vib}^R Q_s(r^R)}\exp[-\Delta G_{eq}^*/k_BT] \\ &= \frac{\omega^R}{2\pi}\exp[-\Delta\bar{G}_{eq}^*/k_BT] \end{aligned} \quad (3.8)$$

where the activation free energy

$$\Delta\bar{G}_{eq}^* = \bar{G}_{eq}(r^*) - \bar{G}_{eq}(r^R) \quad (3.9)$$

contains the solvent entropic terms and ω^R is the r-vibrational frequency of the reactant well located at r^R with free energy value $\bar{G}_{eq}(r^R)$. Most experimental activation free energies are determined via the TST rate in the form[31,32]

$$k = k^{TST}\kappa = (k_BT/h)\exp[\Delta G_{exp}^*/k_BT] \quad (3.10)$$

which in effect defines the experimental activation free energy ΔG_{exp}^*, and where κ is a transmission coefficient associated with recrossing of the transition state to be studied in section 4. On combining eqs 3.8–3.10, we have

$$\Delta G_{exp}^* = \Delta G_{eq}^* - k_BT \ln\left[\kappa\left(\frac{\hbar\omega^R}{k_BT}\right)\frac{\omega_s(r^R)}{\omega_s(r^*)}\right] \quad (3.11)$$

Upon inserting typical values $\kappa \approx 0.5 - 1$ (cf. section 4), $\omega^R \approx 570$ cm^{-1},[33] and again $\omega_s(r^R)/\omega_s(r^*) \sim 1.5$, we find that, within the described framework, ΔG_{exp}^* is smaller than ΔG_{eq}^* by $\lesssim$1 kcal/mol. The very existence of such a difference is generally unappreciated; it is significant in terms of assorted highly detailed activation parameter analyses to be found in the literature,[34,35] although its magnitude is certainly within the errors incurred by our usage of a dielectric continuum model. Such a difference and especially its ingredients would be difficult to sort out experimentally. For a general discussion of the difficulties of dissecting experimental activation parameters, see, e.g., ref 36. Computer simulation[7] could, however, also be used for this purpose. Our numerical estimates for $-\log k$ (k in s^{-1}) are 7.7, 8.6, and 12.3

(29) Notice that a different numerical value for the zeroth-order r- and s-independent solvent frequency ω_s^0 only changes the zero of the reaction free energy $G(r,s)$. In particular, the force constant eq 3.2 and the frequency ratio eq 3.4 are unaffected, since they are not related to the solvent dynamics. The transmission coefficient κ, however, is influenced by ω_s^0 (see section 4 below).

(30) (a) Ogg, R. A., Jr.; Polanyi, M. *Trans. Faraday Soc.* **1935**, *31*, 604. See also: (b) Baughan, E. C.; Evans, M. G.; Polanyi, M. *Trans. Faraday Soc.* **1941**, *37*, 377. (c) Evans, A. G. *Trans. Faraday Soc.* **1946**, *42*, 719.

(31) Glasstone, S.; Laidler, K. J.; Eyring, H. *The Theory of Rate Processes*; McGraw-Hill: New York, 1941. For a modern exposition, see, e.g.: Steinfeld, J. I.; Francisco, J. S.; Hase, W. L. *Chemical Kinetics and Dynamics*; Prentice-Hall: Englewood Cliffs, NJ, 1989.

(32) For an extensive reference list, see ref 1.

(33) Dollish, F. R.; Fateley, W. G.; Bentley, F. F. *Characteristic Raman Frequencies of Organic Compounds*; Wiley: New York, 1974. See also: Williams, R. C.; Taylor, J. W. *J. Am. Chem. Soc.* **1973**, *95*, 1710; the authors used 585 cm^{-1} for ω^R. Grasselli, J. G.; Ritchey, W. M. *Atlas of Spectral Data and Physical Constants for Organic Compounds*; CRC Press: Cleveland, 1975, where $\omega^R = 560$ cm^{-1} is reported.

(34) Abraham, M. H. *J. Chem. Soc., Perkin Trans. 2* **1972**, 1343; *Prog. Phys. Org. Chem.* **1974**, *11*, 1; in *Advances in Solution Chemistry*; Bertini, I., Lunazzi, L., Dei, A., Eds.; Plenum: New York, 1981. Abraham, M. H.; Grellier, P. L.; Nasehzadeh, A.; Walker, R. A. C. *J. Chem. Soc., Perkin Trans. 2* **1988**, 1717.

(35) Koppel, I. A.; Palm, V. A. *Org. React. (Tartu)* **1969**, *6*, 213. Ponomareva, E. A.; Kulik, N. I.; Dvorko, G. F. *Org. React. (Tartu)* **1974**, *11*, 333.

(36) Albery, W. J. *Annu. Rev. Phys. Chem.* **1980**, *31*, 227.

for CH_3CN, C_6H_5Cl, and C_6H_6 solvents, respectively; the corresponding experimental values[34] (estimated from high-temperature data[35] for C_6H_5Cl and C_6H_6) are 8.6, 11.3, and 12.1. The main source of the large -log k discrepancy for C_6H_5Cl is the activation free energy difference of ~3 kcal/mol between the theoretical and experimental estimates (see section 4B of part 1).

4. Transmission Coefficient

We now turn to the transmission coefficient $\kappa = k/k^{TST}$ which measures the deviation of the reaction rate from the conventional equilibrium solvation picture and k^{TST}.[3] The departure from the conventional equilibrium solvation TST rate constant eq 3.8 based on the potential of mean force in eq 3.9 is caused by the following. The reaction route with $\bar{G}_{eq}(r)$ is the ESP in eq 2.6 by construction; the conventional equilibrium solvation theory thus explicitly posits that the solvent orientational polarization maintains its equilibrium with the reactive solute charge distribution during the passage through the transition state. But this full equilibrium postulate is drastically violated in many charge shift reactions;[3-6,7,12,17] in particular, we have seen in section 2 the strong nonequilibrium deviations which occur in the S_N1 ionization reaction path.

In an approximation to be justified below, we neglect the anharmonicity associated with the solvent frequency $\omega_s(r)$, i.e., its r dependence, and calculate κ by employing a simple harmonic model due to van der Zwan and Hynes.[3] In this case, the transmission coefficient κ is given by[3b,c]

$$\kappa = k/k^{TST} = \omega_s/\omega_\perp = \omega_\parallel/\omega_{b,eq} \tag{4.1}$$

where $\omega_\parallel$, $\omega_\perp$ are the normal mode frequencies along and perpendicular to the SRP, and $\omega_{b,eq}$ is the frequency along the ESP projected onto the r coordinate. Most of our discussion below is couched in terms of the first form of eq 4.1. This form is the result of harmonic two-dimensional transition-state theory[37] on the $G(r,s)$ surface. The TST dividing surface is orthogonal to the SRP at the $G(r,s)$ saddle point. In the (r,s) coordinate system, it lies off the s axis and has some r mixed into it. Along this orthogonal coordinate, the (bound) frequency is $\omega_\perp$. On the other hand, the ESP perspective is perhaps most naturally exposed in the $(r,\delta s)$ coordinate system, where $\delta s = s - s_{eq}(r)$.[3b,c,5b,12b] The orthogonal coordinate at the saddle point is defined by $r = r^\ddagger$, i.e., the δs axis. Along this coordinate, the (bound) frequency is ω_s. The ratio $\omega_\perp/\omega_s$ in eq 4.1 reflects just this difference.[38]

As shown by Lee and Hynes,[5b] eq 4.1 can be written as

$$\kappa = \omega_\parallel\left[\omega_{b,na}^2 + \frac{g^2}{\omega_s^2}\right]^{-1/2} = \frac{\omega_\parallel}{\omega_{b,na}}\left[1 + \frac{g^2}{\omega_{b,na}^2\omega_s^2}\right]^{-1/2} \tag{4.2}$$

where $\omega_{b,na}$ is the nonadiabatic barrier frequency "seen" by the solute reaction system at short times,

$$\omega_{b,na}^2 = -\mu_r^{-1}\partial^2 G/\partial r^2|_\ddagger \tag{4.3}$$

calculated with the solvent frozen at $s = s^\ddagger$, and g is the solute–solvent coupling

$$g = \frac{1}{\sqrt{\mu_s\mu_r}}\frac{\partial^2 G}{\partial s\partial r}\bigg|_\ddagger = -2\frac{\Delta G_r}{\sqrt{\mu_s\mu_r}}\frac{\partial c_f^2}{\partial r}\bigg|_\ddagger \tag{4.4}$$

where we have used eqs 2.4, 2.5, and 2.7 in going from the second to the last member. Equation 4.4 explicitly shows that the solute–solvent coupling depends upon the S_N1 electronic structure variation along the RX separation coordinate r, in a fashion similar to the solvent force constant K_s in eq 3.2. All the frequencies in eqs 4.1–4.4 are evaluated at the transition state, which is a saddle point on the free energy surface. The normal mode frequencies $\omega_\parallel$ and $\omega_\perp$ can be expressed in terms of $\omega_{b,na}$, ω_s, and g as[3b,c,5b]

$$-\omega_\parallel^2 = \frac{1}{2}\left\{(\omega_s^2 - \omega_{b,na}^2) - (\omega_s^2 + \omega_{b,na}^2)\left[1 + \frac{4g^2}{(\omega_s^2 + \omega_{b,na}^2)^2}\right]^{1/2}\right\}$$

$$\omega_\perp^2 = \frac{1}{2}\left\{(\omega_s^2 - \omega_{b,na}^2) + (\omega_s^2 + \omega_{b,na}^2)\left[1 + \frac{4g^2}{(\omega_s^2 + \omega_{b,na}^2)^2}\right]^{1/2}\right\} \tag{4.5}$$

Table I. Calculated Frequencies for S_N1 Ionization[a,b]

	ω_2	$\omega_\perp$	$\omega_\parallel$	$\omega_{b,eq}$	$\omega_{b,na}$	$\sqrt{-g}$
C_6H_5Cl	13.1	16.1	62.5	77.1	61.8	24.5
CH_3CN	11.1	17.0	70.8	108.7	69.6	30.4

[a] Unit: ps^{-1}. [b] Transition (and reactant) state separations are given in paper 1, section 4B.

Equation 4.2 is the expression for κ originally derived via Grote–Hynes theory[39] by van der Zwan and Hynes[3] in the nonadiabatic frozen solvent limit,[3-5,12] and should be appropriate for S_N1 reactions.[4,5] Our model calculations based on the (equivalent) first member of eq 4.1 yield $\kappa \approx 0.65$ for t-BuCl ionization in CH_3CN and $\kappa \approx 0.81$ for C_6H_5Cl. For the former case especially, this is a noticeable departure from the equilibrium solvation TST prediction. It is worth remarking that a κ value in this range has been found in a molecular dynamics computer simulation of a model for the t-BuCl ionization in water by Keirstead et al.,[7] as has the applicability of eq 4.1. It is instructive to note that, by contrast, Kramers' theory[40] incorrectly predicts[7] a very much smaller κ value ≈0.019, a general feature anticipated in ref 4.

The results for the transmission coefficient can be understood in several ways. The first form in eq 4.1 is,[3,5] as noted above, a generalized variational transition-state[3,5,10,11] perspective, in which the solvent lagging of the t-BuCl ionization r-motion is accounted for by following the passage over the barrier along the true reaction coordinate, the SRP (albeit in the harmonic approximation); along this path there are no recrossings. The second form in eq 4.1, as well as eq 4.2, arises from a one-dimensional perspective along r in which recrossings of the transition state at $r^\ddagger$ are accounted for by dynamical solvent time-dependent frictional effects according to the Grote–Hynes theory,[39] which has proved successful in accounting, for example, for computer simulations of a wide range of reaction classes[7,12a-c,17,41-43] and in the interpretation of experimental rates;[44] indeed eq 4.2 is the nonadiabatic solvation limit of that theory, involving the initial time value of the time-dependent friction. In that description, the supposed reaction path is along the ESP, projected onto the single dimension r, so that the picture is that of motion along the potential of mean force; then nonequilibrium solvation leads to a solvent friction and is responsible for recrossings and a concomitant κ value less than unity; equivalently, the reactive frequency $\omega_\parallel$ is less than the equilibrium barrier frequency $\omega_{b,eq}$. The connection between the two perspectives (including the coordinate rotation necessary to interconvert them) is discussed in more detail in refs 3, 5, and 12b.[45]

(37) See refs 8-11 for a discussion for reactions in the gas phase.

(38) Since $s_{eq}(r)$ is a function of r, there is a nonorthogonal transformation between $(r, \delta s)$ and (r, s), so that the dividing surface $r = r^\ddagger$ in the $(r, \delta s)$ system maps into the surface $r = r^\ddagger$ in the (r, s) plane, rather than being orthogonal to the line $s = s_{eq}(r)$ in that plane. See refs 3, 5, and 12b,f for further discussion.

(39) Grote, R. F.; Hynes, J. T. *J. Chem. Phys.* **1980**, *73*, 2715.
(40) Kramers, H. A. *Physica* **1940**, *7*, 284.
(41) Bergsma, J. P.; Reimers, J. R.; Wilson, K. R.; Hynes, J. T. *J. Chem. Phys.* **1986**, *85*, 5625.
(42) Zichi, D. A.; Ciccotti, G.; Hynes, J. T.; Ferrario, M. *J. Phys. Chem.* **1989**, *89*, 2093.
(43) Zhu, S. B.; Lee, J.; Robinson, G. W. *J. Phys. Chem.* **1988**, *92*, 2401. Berne, B. J.; Borkovec, M.; Straub, J. E. *J. Phys. Chem.* **1988**, *92*, 3711. Roux, B.; Karplus, M. *J. Phys. Chem.* **1991**, *95*, 4856.
(44) Bagchi, B.; Oxtoby, D. W. *J. Chem. Phys.* **1983**, *78*, 2735. Ashcroft, J.; Besnard, M.; Aquada, V.; Jonas, J. *Chem. Phys. Lett.* **1984**, *110*, 430. Zeglinski, D. M.; Waldeck, D. H. *J. Phys. Chem.* **1988**, *92*, 692. Sivakumar, N.; Hoburg, E. A.; Waldeck, D. H. *J. Chem. Phys.* **1989**, *90*, 2305. Park, N. S.; Waldeck, D. H. *J. Phys. Chem.*, in press. McManis, G. E.; Weaver, M. J. *J. Chem. Phys.* **1989**, *90*, 1720.

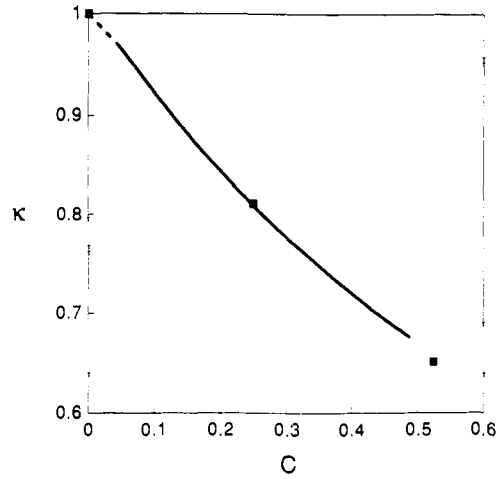

Figure 5. Transmission coefficient versus the solvent polarity factor $C = \epsilon_\infty^{-1} - \epsilon_0^{-1}$. For simplicity, we have assumed in the numerical calculation (denoted as —) that $\epsilon_\infty = 2$; the dashed line is the smooth extrapolation to $C = 0$, made due to an instability in the numerical calculation for very small C. Transmission coefficients for benzene ($\epsilon_0 = 2.27$), chlorobenzene ($\epsilon_\infty = 2.33$, $\epsilon_0 = 5.62$), and acetonitrile ($\epsilon_\infty = 1.81$, $\epsilon_0 = 35.94$) solvents are marked by filled squares.

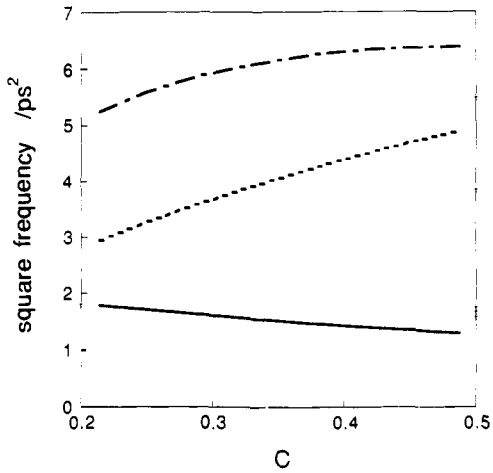

Figure 6. Solvent and nonadiabatic barrier square frequencies versus the solvent polarity factor C: (—) $\omega_s^2/10^2$, (···) $\omega_{b,na}^2/10^4$, (- · - · -) $\omega_{b,na}^2\omega_s^2/10^6$. Because of the linear behavior of decreasing ω_s^2 and increasing $\omega_{b,na}^2$ with C, the product $\omega_{b,na}^2\omega_s^2$ is a parabolic function of C and varies little in a wide range of solvent polarity ($3 \lesssim \epsilon_0 \lesssim 80$).

As illustrated in more detail below, there is a strong electrostatic coupling between the S_N1 solute and the solvent, especially for high polarity. The reason that κ is so close to unity *despite* the strength of the solute–solvent coupling inducing recrossing (and despite the large nonequilibrium solvation effects apparent in the reaction path) is the sharpness of the barrier, e.g., $\omega_{b,na} \sim 70$ ps^{-1} (Table I). This provides a strong local driving force favoring product formation, and solvent-induced recrossings occur only to a modest extent even though the solvent is nearly "frozen".[3,5,12]

We now turn to a general examination of the κ variation with solvent polarity. The result obtained by using the first member of eq 4.1 with $\omega_s^0 = 15$ ps^{-1} is displayed in Figure 5 versus the (Pekar) solvent polarity factor C

$$C \equiv \frac{1}{\epsilon_\infty} - \frac{1}{\epsilon_0} \tag{4.6}$$

As the solvent polarity C increases, so does the solvent reorganization free energy $\Delta G_r^\ddagger$ at the transition state via eq 2.2, since the transition-state location $r^\ddagger$ changes little with C (cf. Figure 8a of part 1). In fact, $\Delta G_r^\ddagger$ at the transition state and the solvent polarity C are almost proportional to each other. Accordingly, hereafter we will use them interchangeably. We find a monotonically decreasing transmission coefficient with increasing solvent reorganization free energy $\Delta G_r^\ddagger$ at the transition state and thus with the solvent polarity.

In order to analyze κ, we will employ eq 4.2. We can first simplify this somewhat; since by numerical calculation $\omega_{b,na}^4 \gg g^2, \omega_s^4$ for the sharp barrier *t*-BuCl reaction (Table I), we can expand the parallel frequency $\omega_\parallel$ in eq 4.5 to obtain

$$\omega_\parallel^2 \approx \omega_{b,na}^2\left[1 + \frac{g^2}{\omega_{b,na}^4}\right] \tag{4.7}$$

which, when substituted into eq 4.2, yields

$$\kappa \approx \left[1 + \frac{g^2}{\omega_{b,na}^4}\right]^{1/2}\left[1 + \frac{g^2}{\omega_{b,na}^2\omega_s^2}\right]^{-1/2} \tag{4.8}$$

A further consistent simplification is possible. Since $g^2/\omega_{b,na}^4 \lesssim 0.03$ according to numerical calculations for a wide range of solvent polarity (Table I), the transmission coefficient change with C is mainly determined by the second term in the second bracket of eq 4.8

$$\kappa \approx \left[1 + \frac{g^2}{\omega_{b,na}^2\omega_s^2}\right]^{-1/2} \tag{4.9}$$

In order to analyze the solvent polarity dependence of this, we first consider the denominator in eq 4.9, i.e., the solvent frequency ω_s and the nonadiabatic barrier frequency $\omega_{b,na}$. As shown by the numerical calculations displayed in Figure 6, ω_s^2 decreases monotonically and linearly with the solvent polarity factor C, while $\omega_{b,na}^2$ grows with C. The diminishing solvent frequency arises from the feature that the solvent inertia μ_s increases (the solvent appears more massive), with the solvent reorganization free energy $\Delta G_r^\ddagger$ (eq 3.5) and thus with C (The corresponding increase in K_s is not as rapid, due to solute polarizability.[28]). The $\omega_{b,na}$ behavior is associated with the fact that at the diabatic crossing point between the ionic and covalent curves in solution, the ionic slopes steepen with increasing C (cf. Figure 9 of part 1); this results in a larger curvature when the smooth ground-state surface is obtained by taking into account the electronic coupling term β. Owing to these opposite trends, the product $\omega_{b,na}^2\omega_s^2$ does not depend very strongly on the solvent polarity.[46] Figure 6 shows that the relative change in the product is $\lesssim$25% for a wide range of solvent polarity ($3 \lesssim \epsilon_0 \lesssim 80$). The major factor in the κ variation with C then is the solute–solvent coupling g in eq 4.9, which explicitly depends upon how the S_N1 solute electronic structure changes as the system passes through the transition state (cf. eq 4.4). We discuss this next.

In analyzing the solute–solvent coupling g, we will focus our attention on the higher solvent polarity regime, since it is here that κ is smallest. From eq 4.4, this requires calculation of the variation of the delocalization variable x, eq 2.5, with respect to the RX separation coordinate r. By differentiating eq 2.4 with respect to r, using the relation $x\partial x/\partial s + y\partial y/\partial s = 0$ derived from the normalization condition eq 2.5, and utilizing the equilibrium condition eq 2.7, we find

$$-\left.\frac{\partial x}{\partial r}\right|_{eq} = 2\left.\frac{\partial c_I^2}{\partial x}\right|_{eq} \simeq y\frac{y(V_C^{0\prime} - V_I^{0\prime} + \Delta G_r^{el\prime} + 2\Delta G_r^\ddagger{}'s) - \frac{1}{2}x(\rho\Delta G_r^{el})' + 2x\beta'}{2y\beta - x(V_C^0 - V_I^0 + \Delta G_r^{el} + 2\Delta G_r^\ddagger s) - \frac{1}{2}y\rho\Delta G_r^{el}}\Bigg|_{eq} \tag{4.10}$$

(45) An extension of aspects of the (linear) variational transition-state treatment of ref 3 to include many harmonic coordinates is given in: Pollak, E. *J. Chem. Phys.* **1986**, *85*, 865. For subsequent work, see: Pollak, E. *J. Chem. Phys.* **1991**, *95*, 533 and references therein.

(46) This is rather interesting in that the solvent mass effect associated with μ_s, realized as diminishing solvent frequency with growing C, is almost completely offset by the nonadiabatic barrier frequency $\omega_{b,na}$. This cancellation was not noticed in the classical analysis.[3-5]

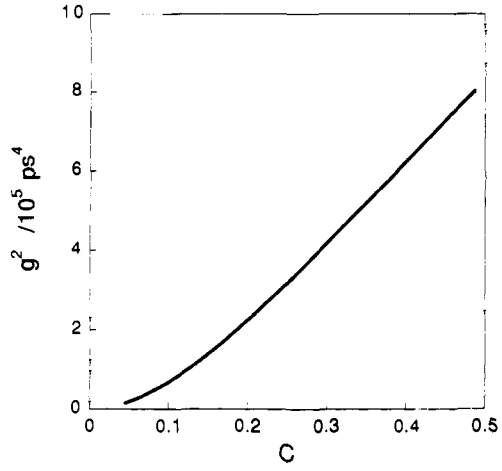

Figure 7. Solute–solvent coupling g, eq 4.4, versus the solvent polarity factor C.

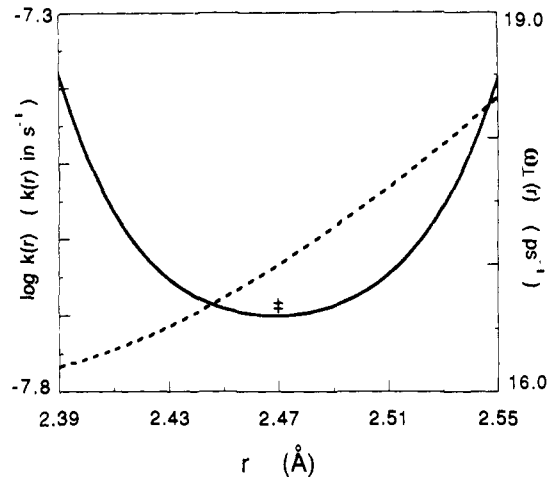

Figure 8. Rate constant and transverse frequency in eq 4.13 versus r in CH_3CN: (—) log $k(r)$, (···) $\omega_\perp(r)$. The variation in the frequency transverse to the SRP, $\omega_\perp(r)$, does not induce a change in the transition-state location. The r value of the minimum in log $k(r)$ is the same as that of the saddle point, $r^\ddagger \approx 2.47$ Å.

where V_C^0, V_I^0, and β are the diagonal and off-diagonal elements of the vacuum Hamiltonian for t-BuCl in eq 2.1, and ΔG_r^{el}, ΔG_r are the solvent reorganization free energies, eq 2.2, associated with solvent electronic and orientational polarizations. Here $'$ denotes an ordinary r derivative. As shown in part 1, especially Figure 8b there, the transition state is rather delocalized except for weakly polar solvents ($\epsilon_0 \lesssim 10$) so that $x \approx 0, y \approx 1$ (cf. eq 2.5). Equation 4.10 then reduces to a simpler form at the transition state:

$$\left.\frac{\partial c_I^2}{\partial r}\right|_\ddagger \approx \left.\frac{V_C^{0\prime} - V_I^{0\prime} + \Delta G_r^{el\prime} + \Delta G_r'}{4\beta - \rho\Delta G_r^{el}}\right|_\ddagger \qquad (4.11)$$

Our model t-BuCl system is characterized by a rather large electronic coupling ($\beta \approx 15$–18 kcal/mol) in the transition region $2.4 \text{ Å} \lesssim r \lesssim 2.7$ Å (thus $\rho \approx 0.3$–0.4 with $\hbar\omega_{el} \sim 4$ eV), while $\Delta G_r^{el} \approx 15$–$18$ kcal/mol for $\epsilon_\infty = 2$ (cf. section 5 of part 1); thus the denominator in eq 4.11 is always positive and remains nearly constant except for weakly polar solvents. The numerator is also positive, since the diabatic ionic potential V_I^0 is a decreasing function (Figure 4 of part 1), while both the covalent curve V_C^0 (Figure 4 of part 1) and the solvent reorganization free energies ΔG_r^{el}, ΔG_r (cf. Figure 4a) decrease in the transition-state region. Therefore, $\partial c_I^2/\partial r|_\ddagger > 0$; the ionic character of t-BuCl increases as the RX bond stretches farther from its transition-state bond length $r^\ddagger$ with the solvent coordinate fixed at its transition-state value $s^\ddagger$. This agrees with the charge evolution along the two reaction paths shown in Figure 3, although the solvent coordinate s is allowed to change with r there (rather than remain fixed). We also notice here that the solvent orientational polarization term $\Delta G_r'$ in eq 4.11 is at best one-half of the entire solvent contribution. Moreover, the r-gradients of the vacuum diabatic potentials are much larger in magnitude than the solvation term. Therefore, we conclude that $\partial c_I^2/\partial r|_\ddagger$ is nearly independent of the solvent reorganization free energy ΔG_r and thus the solvent polarity factor C, except for weakly polar solvents ($\epsilon_0 \lesssim 10$) where the $r^\ddagger$ variation with C has a more pronounced effect.

Since the solvent mass is proportional to ΔG_r via eq 3.6, we find from eqs 4.4 and 4.11 that the solute–solvent coupling g is negative and

$$g^2 = \frac{2\omega_s^{0\,2}\Delta G_r}{\mu_r}\left[\left.\frac{\partial c_I^2}{\partial r}\right|_\ddagger\right]^2 \qquad (4.12)$$

Since by our discussion above the ionic character gradient term in the bracket depends rather weakly on the reorganization free energy ΔG_r and thus on the solvent polarity factor C (at least for highly polar solvents), we can conclude that $g^2 \propto \Delta G_r$, which is confirmed numerically in Figure 7. In fact, the magnitude of the solute–solvent coupling g increases as a square root of C in almost the entire solvent polarity range ($3 \le \epsilon_0 \le 80$) investigated numerically. Thus the more polar the solvent is, the larger is the solute–solvent coupling; for example, the g ratio between CH_3CN and C_6H_5Cl is calculated to be about 1.5 (Table I). We naturally expect that a successful reactive trajectory involves at the transition state more solvent motion for highly polar solvents due to a larger solute–solvent coupling than for weakly polar solvents. This results in the observed decrease in the transmission coefficient with solvent polarity.[47-49]

Finally, we can also calculate the reaction rate based on a fully nonlinear variational transition-state treatment,[5] where the harmonic approximation is not made. For the same reason as encountered in the $\bar{G}_{eq}$ calculation in section 3, i.e., the strong inhomogeneity in $\omega_s(r)$ due to the quantum mixing of covalent and ionic states, the transverse mode frequency $\omega_\perp$ in eq 4.1 also varies

(47) To see how sensitive κ is to ω_s^0, we compare the transmission coefficients for two different values, 15 ps^{-1} and 30 ps^{-1}, for ω_s^0. Since neither the force constant K_s nor the reorganization free energy ΔG_r is affected by ω_s^0,[29] the solvent mass associated with $\omega_s^0 = 30$ ps^{-1} is four times smaller than that for $\omega_s^0 = 15$ ps^{-1} for any given r via eq 3.6. We thus would expect the transmission coefficient with $\omega_s^0 = 30$ ps^{-1} to be larger than that with $\omega_s^0 = 15$ ps^{-1} due to a diminished inertial effect. The numerical results confirm this, although what accounts for this increase in κ is *not* the solvent inertia as explained below. Another interesting feature is that the relative κ increment is very small (less than 4%) while the solvent mass μ_s is reduced by a factor of 4 and the solvent frequency ω_s is doubled. Equations 3.4 and 4.12 may be the most revealing on this. Both the square solvent frequency ω_s^2 and the solute–solvent coupling g scale the same way when we change ω_s^0, i.e., they grow as $\omega_s^{0\,2}$. Therefore the inertial effect associated with ω_s^2 is exactly cancelled by g in the second square bracket of eq 4.8. Thus the observed ~4% increase in κ arises from the first bracket term in eq 4.8; the increase in the solute–solvent coupling g rather than the reduced solvent inertia is responsible for the transmission coefficient change.

(48) In the nonadiabatic solvation limit,[3-5,12] the solute–solvent coupling g is related to the initial time value of the time-dependent friction $\zeta(t)$ in the one-dimensional generalized Langevin equation associated with the motion along r by $\zeta(0) = g^2/\omega_s^2$ (refs 3, 4, and 39). For the high solvent polarity case, an approximate analytic expression for ω_s is available with an assumption of a delocalized transition state using manipulations similar to those for g in section 4:

$$\omega_s^2 \approx \left[1 - \frac{2\Delta G_r}{4\beta - \rho\Delta G_r^{el}}\right]\omega_s^{0\,2}$$

This yields the initial friction approximation

$$\zeta(0) \approx \frac{2\Delta G_r}{\mu_r}\,\frac{(V_C^{0\prime} - V_I^{0\prime} + \Delta G_r^{el\prime} + \Delta G_r')^2}{(4\beta - \rho\Delta G_r^{el})(4\beta - \rho\Delta G_r^{el} - 2\Delta G_r)}$$

Since g^2 increases linearly with C (Figure 7) while ω_s^2 is an almost linearly decreasing function (Figure 6), the initial friction value $\zeta(0)$ grows in a hyperbolic fashion with solvent polarity. Numerical calculations confirm this.

(49) The nonadiabatic solvation frozen solvent limit discussed here will typically not apply for broad barrier reactions, for which the solvation dynamics *per se* will play an important role.[3,4,12a,c,17]

along the SRP; the notation $\omega_\perp(r)$ is thus appropriate.[5a] To see how this might affect the reaction picture, we follow Lee and Hynes[5b] and consider a rate-like expression $k(r)$ defined at each point (r, s) on the SRP:

$$k(r) = \frac{k_B T}{h} \frac{Q_\perp(r)}{Q_\parallel^R Q_\perp^R} \exp\left[-\frac{G^{SRP}(r) - G_R}{k_B T}\right] \quad (4.13)$$

Here $Q_\parallel^R$ and $Q_\perp^R$ are, respectively, the functions associated with the two normal modes parallel and perpendicular to the SRP at the reactant state, and $Q_\perp(r)$ is the partition function for the transverse mode at a point (r, s) on the SRP. The corresponding free energies are G_R and $G^{SRP}(r)$, respectively.[50] In the nonlinear variational transition-state theory,[5] the reaction rate is determined by the minimum value of $k(r)$. (This is strictly analogous to the procedure carried out in gas-phase variational TST studies.[9-11]) Because of the inhomogeneity in $\omega_\perp(r)$ and the associated entropy effect, this minimum may not occur at the saddle point (r^*, s^*) on the free energy surface; it rather could be shifted to a different r value owing to the competition between G^{SRP}, which favors the standard transition state, and entropic contributions associated with $\omega_\perp(r)$, which favor a displaced transition state. To explore this possibility, we have numerically scanned the local region near the saddle point following the SRP and have calculated $k(r)$, evaluating the partition functions classically. Figure 8 shows the result, as well as the local behavior of $\omega_\perp(r)$, for CH_3CN. The r range was ± 0.08 Å so that $G^{SRP}(r)$ was within $\sim k_B T$ of the saddle point, and the step size was 1×10^{-5} Å. $\omega_\perp(r)$ increases with r in the saddle point region because of the increasing angle of the SRP relative to the r axis (cf. Figure 1a). This results in more of a contribution from the higher frequency r motion, although clearly the s contribution is dominant. It can be seen from Figure 8 that although $\omega_\perp(r)$ is not constant, the minimum in $k(r)$ corresponds to the same saddle point value that we have employed heretofore. Thus as for the potential of mean force and $\omega_s(r)$, the inhomogeneity in $\omega_\perp(r)$ plays no significant role, a conclusion consistent with that of ref 5a. In particular, the transition-state location is not sensitive at room temperature to the entropic contributions because of the moderate variation of $\omega_\perp(r)$; this is in contrast[5a] to high-temperature gas-phase reactions where analogous frequency variations can lead to marked variational transition-state shifts,[9,11] a reflection of the greater importance of entropy at higher temperatures. This ensures that the transmission coefficient obtained from eq 4.1 is indeed a valid measure for the deviation from the conventional equilibrium solvation theory.

(50) Since the SRP is a single-valued curve in (r, s) coordinates, the r value completely specifies a location on the SRP.

5. Concluding Remarks

In this paper, we have used the electronic structure-based two-dimensional free energy formulation of part 1 to find that there is significant deviation from the equilibrium solvation path for a model of the *t*-BuCl S_N1 ionization in solution. This deviation arises from a solvent lag as the system crosses the transition state, as indicated by the disparity between the solution reaction path and the equilibrium solvation path. This lag occurs despite the strong solute–solvent coupling, proportional to the change of the S_N1 solute ionic character with the nuclear separation.

With the aid of linear and nonlinear variational transition-state theory, we have predicted that these nonequilibrium solvation effects can lead to marked departures of the rate constant from its equilibrium solvation transition-state theory approximation, especially for more polar solvents. This leads to a solvent polarity dependence of the rate over and above that due to the true activation free energy. In addition to their intrinsic interest as indicators of dynamic solvent-induced transition-state recrossing and deviations from the equilibrium solvation path, such departures which depend on the solvent polarity, can contribute factors of ≈ 1 kcal/mol to the apparent free energy of activation. This is not an insignificant effect in terms of the detailed level of activation free energy analysis often presented in the literature for S_N1 reactions.[34,35]

We expect that reaction path and rate features similar to those that we have found will also arise in other reaction classes such as twisted intramolecular charge transfer[51,52] and photoionizations,[53] where significant charge variation occurs along nuclear coordinates due to electronic mixing involving ionic states.

Finally, many of the features described here are confirmed in an application of a variant of our formulation to a microscopic level molecular dynamics simulation of a model of the *t*-BuCl S_N1 ionization in water.[7]

Acknowledgment. This work was supported in part by NSF Grant CHE88-07852. We thank Dr. W. Keirstead and Professor K. R. Wilson for useful discussions concerning the potential of mean force.

Registry No. *t*-BuCl, 507-20-0.

(51) Barbara, P. F.; Kang, T. J.; Jarzeba, W.; Fonseca, T. In *Perspectives in Photosynthesis*; Jortner, J., Pullman, B., Eds.; Kluwer: Dordrecht, 1990. Barbara, P. F.; Jarzeba, W. *Adv. Photochem.* **1990**, *15*, 1.

(52) Kim, H. J.; Hynes, J. T. *Solute Electronic Structure and Solvation in Time-Dependent Fluorescence: I. Formulation and Application to a Two-State Model*, to be submitted for publication. Kim, H. J.; Simon, J. D.; Hynes, J. T. *Solute Electronic Structure and Solvation in Time-Dependent Fluorescence: II. Three-State Model*, to be submitted for publication.

(53) See, for example: Goodman, J. L.; Peters, K. S. *J. Am. Chem. Soc.* **1985**, *107*, 6459. Spears, K. G.; Gray, T. H.; Huang, D.-Y. *J. Phys. Chem.* **1986**, *90*, 779.

Spin Preferences of Conjugated Polyradicals: The Disjoint NBMO Analysis

Julianto Pranata

Contribution from the Department of Chemistry and Biochemistry, University of Arkansas, Fayetteville, Arkansas 72701. *Received April 24, 1992*

Abstract: The concept of disjoint nonbonding molecular orbitals (NBMOs) has been extended from its original application to biradicals to molecules with more than two NBMOs. It is shown how the disjointness of NBMOs in polyradicals can be related to their spin preferences. Ab initio molecular orbital calculations are reported which demonstrate the validity of the disjoint NBMO analysis.

In 1977 Borden and Davidson introduced the concept of disjoint nonbonding molecular orbitals (NBMOs) and showed how this concept can be used to rationalize the ground-state spin preferences of conjugated biradicals—molecules possessing two NBMOs

0002-7863/92/1514-10537$03.00/0